2022 9th IEEE RAS/EMBS International Conference for Biomedical Robotics and Biomechatronics (BioRob) | 978-1-6654-5849-8/22/$31.00 ©2022 IEEE | DOI: 10.1109/BIOROB52689.2022.9925393

A Data-based Approach to Simultaneously Align Local and Global Frames between an Inertial Measurement Unit (IMU) and an Optical Motion Capture System

Yichu Jin*, Yu Meng Zhou*, Connor M. McCann, Tommaso Proietti, Chris H. Rycroft, Conor J. Walsh

***Abstract*— Motion tracking algorithms using inertial measurement units (IMU) are commonly evaluated against ground truth measurements from optical motion capture systems (OMC). A fair comparison between IMU and OMC requires accurate frame alignment between the two systems. Existing methods address the local and global frame misalignments as separate issues, either relying on various assumptions or precise calibration measurements. In this work, we propose an assumption-free data-based method that simultaneously aligns both local and global frames via quaternion-based least squares optimization. For performance evaluation, we compared the proposed method with methods based on commonly accepted assumptions. Using human kinematics data from 6 participants, the proposed method produced the best alignment results with error less than 1.5° and its error profile was the least correlated with motion. We then conducted sensitivity analysis on input data characteristics and showed the necessity of using data with sufficient range of motion to ensure alignment accuracy. Lastly, we demonstrated that the proposed method could be used for isolating IMU drift during dynamic movements. The proposed alignment method could serve as a valuable tool for developing and evaluating IMU-based motion tracking algorithms.**

I. Introduction

Analyzing human movements in the real-world environment is important in many applications, including rehabilitation, ergonomics, entertainment, and human performance augmentation [1]–[5]. Inertial measurement units (IMUs) have been one of the most commonly used wearable sensors for motion tracking outside lab-based environments, as they are easily portable, lightweight, and simple to attach to the body. IMUs fuse gyroscope, accelerometer, and magnetometer signals to estimate 3D orientations. Joint kinematics can then be estimated by comparing relative orientations of IMUs attached to adjacent body segments. Kinematic estimation methods using IMUs have constantly been advancing, with specific topics ranging from algorithmic breakthroughs (e.g., rejecting magnetic disturbances [6]–[9]) to practical guidelines (e.g., robust calibration routines [10], [11]). Although there exists an abundance of developments in IMU algorithms, often there is a lack of clarity on evaluation methods to compare an IMU orientation estimate to a ground truth reference, often an optical motion capture system (OMC).

This work was supported by the Tata-Harvard Alliance, National Science Foundation (EFRI Award No. 1830896, Graduate Research Fellowship No. DGE1745303).

All authors are affiliated with John A. Paulson School of Engineering and Applied Sciences, MA 02139 USA. Corresponding author email: walsh@seas.harvard.edu

*These authors contributed equally to this work.

The process of comparing IMU orientation to a ground truth reference is crucial for algorithm development and surprisingly not trivial. The key challenge of orientation comparison comes from the fact that IMUs and OMCs describe orientations in terms of different coordinate frames [12], [13]. In geometry, orientations are expressed as rotation of a local coordinate relative to a global reference frame. IMU and OMC measure *different* local frame orientations with respect to *different* global references, hence any mismatch in either their local or global coordinate frames can significantly affect kinematics tracking and evaluation accuracy [14], [15].

The local and global frames of IMU and OMC are not the same due to the differences in their definitions, calibration, and measurement methods. Local frames of IMUs are defined by the orientations of their sensing chips, with the axes aligned to the geometry of the chips. On the other hand, local frames of OMCs are defined by any group of 3 or more rigidly mounted reflective markers. These markers have been placed on human body segments to act as trackers for anatomical coordinate frames [16], [17] or sometimes directly coupled with IMU cases to validate IMU-based algorithms [11], [18]. The global frames of IMUs are defined using the direction of gravity and the heading of the Earth's magnetic field, whereas global frames of OMCs are usually aligned with the walls or the floor tiles of the motion capture lab. Therefore, as IMU and OMC measure orientations with different local and global frames, alignment of these frames is essential for reliable comparisons.

As a highly prevalent issue, IMU to OMC frame alignment has been explored using a range of approaches, from manual to algorithmic. However, current methods rely on various assumptions and treat global and local frame alignments as two standalone issues. In existing approaches, global frames could be aligned by representing the IMU global frame in the OMC global frame by estimating the gravity vector [19] and the Earth's magnetic field [20]. An alternative method places OMC markers directly on the IMU case and assumes that the two measurement systems have identical local frames. With this assumption, global frames can then be aligned mathematically [21]. However, perfect alignment between an IMU and its case cannot be guaranteed; for instance, Xsens MTw, one of the most commonly used IMUs for kinematics tracking, could have up to 3° of sensor-to-case misalignment [22]. Without assuming perfect sensor-to-case alignment, local frames have been aligned algorithmically by matching angular velocities [19], [23] or gyroscopic angles [24]. However, these

methods are evaluated against manually-measured local frame misalignment values and do not consider any global frame mismatch.

Although there exist several solutions to IMU and OMC frame misalignment, current approaches either use assumptions running the risk of oversimplifying or require specific calibration procedures that involve precise measurements. There is an opportunity to expand upon existing work with an accurate method that is assumption-free and only requires simple calibration.

In this work, we address this gap by proposing a simultaneous alignment method (SAM) that can solve for both global and local alignment rotations using a data-based approach. First, we formulate the problem as a quaternion-based least squares optimization. Second, we use arm movement data from 6 participants to evaluate the method and compare it against custom methods based on generally accepted assumptions. Third, we conduct a sensitivity analysis to assess the effect of input data's range of motion on the method performance. Finally, we demonstrate that this method can be applied to isolate and thus better visualize IMU drift during dynamic motion, a challenging issue that hinders validation of IMU-based kinematic estimators [12], [25], [26]. Our proposed alignment method can be used by the research community when designing and evaluating kinematics tracking algorithms for real world applications.

II. Problem Definition

To understand this frame alignment problem, a representative scenario is illustrated in Fig. 1. In this scenario, an IMU is rigidly mounted to a body-worn, 3D-printed case with OMC markers attached. The IMU local frame (IL) is defined by the physical placement of the sensing chip. The IMU global frame (IG) is defined using gravity and the magnetic north. The OMC local frame (OL) is defined by the markers on the IMU case, and the OMC global frame (OG) is defined using a calibration tool. A calibration tool, like the illustrated L-frame, is commonly used in OMC systems and usually placed flat on the ground in alignment with floor tiles or walls for cameras to register it as the OMC global coordinate system [27].

Mathematically, the IMU's local and global frames are related to those of the OMC system through

$$R_{OL}^{OG} = R_{IG}^{OG} R_{IL}^{IG} R_{OL}^{IL} \tag{1}$$

where R denotes the rotation of the subscript coordinate frame expressed in the superscript coordinate frame. Out of the 4 rotation matrices in Eq.1, R_{OL}^{OG} and R_{IL}^{IG} are measurable and represent outputs from the OMC and the IMU respectively. The other two matrices, R_{IG}^{OG} and R_{OL}^{IL} are the unknown misalignment rotations that need to be found:

- R_{IG}^{OG} represents the unknown global frame misalignment between the two systems. Generally, most of the global misalignment is around the yaw axis. This is because the yaw axes from both systems are usually defined using gravity. Yet, the roll and pitch axes are not aligned when the L-frame does not point directly towards the magnetic north.
- R_{OL}^{IL} represents the unknown local frame misalignment. In the scenario described in Fig. 1, R_{OL}^{IL} represents the mechanical misalignment between the IMU chip and the markers mounted on its case. This alignment rotation is expected to be constant over time given that the IMU is rigidly attached to its case.

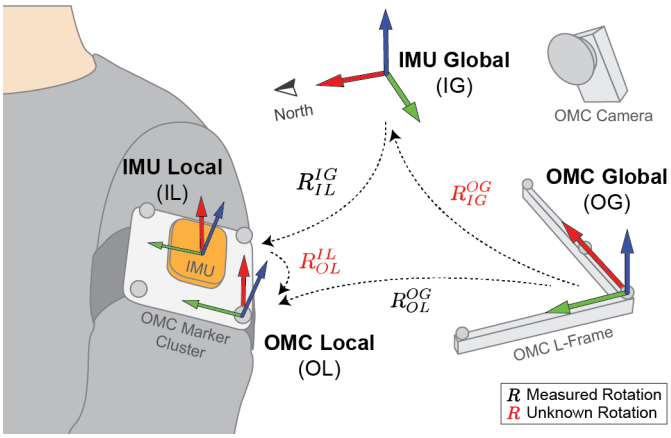

Fig. 1. Illustration of the local (OL, IL) and global (OG, IG) frames of an OMC and a body-worn IMU. R_{OL}^{OG} and R_{IL}^{IG} represent the OMC and IMU rotation measurements respectively. R_{IG}^{OG} and R_{OL}^{IL} denote the unknown global and local frame misalignment between the two systems respectively.

III. Alignment Methods

A. Proposed Method (SAM)

In this section, we introduce the simultaneous alignment method (SAM), a quaternion-based least squares optimization method for simultaneously aligning the local and global frames of IMU and OMC. Given that IMU and OMC measurements are related by Eq. 1, the goal is the solve for the unknown misalignments, R_{IG}^{OG} and R_{OL}^{IL}, that best satisfy

$$R_{OL,t}^{OG} = R_{IG}^{OG} R_{IL,t}^{IG} R_{OL}^{IL} \quad \forall t \in [0, T] \tag{2}$$

for a duration of time. $R_{OL,t}^{OG}$, $R_{IL,t}^{IG}$ represent time series data of OMC and IMU measurements respectively and T represents the total duration of the data.

To formulate Eq. 2 into a least squares optimization, we first convert the rotation matrices into unit quaternions by defining

$$\begin{aligned} u_t &= R_{OL,t}^{OG}, & w_t &= R_{IL,t}^{IG}, \\ a &= (R_{OL}^{IL})^{-1}, & b &= R_{IG}^{OG}. \end{aligned} \tag{3}$$

Then Eq. 2 can be written into quaternion representation:

$$u_t a = b w_t \quad \forall t \in [0, T]. \tag{4}$$

Eq. 4 can be expressed as a least squares problem with the residual function

$$\rho = \sum_{t=0}^{T} \| u_t a - b w_t \|^2 \tag{5}$$

where $\|q\|$ represents the L-2 norm of a quaternion q. The residual function in Eq. 5 can then be simplified into

$$\rho = 2(T+1) - 2\sum_{t=0}^{T}[bw_t a^* u_t^*]_S \tag{6}$$

where $[q]_S$ denotes the scalar component of quaternion q, and a^*, u_t^* represent the conjugates of a and u_t respectively. For the full derivation of Eq. 6, please refer to the appendix.

For this work, Eq. 6 was minimized numerically using MATLAB's `fmincon` function with the sequential quadratic programming optimization algorithm. Additionally, nonlinear equality constraints of

$$\|a\| = 1, \quad \|b\| = 1 \tag{7}$$

are required to ensure the resulting a and b are unit quaternions. The optimal alignment rotations R_{OL}^{IL} and R_{IG}^{OG} can then be found by converting a and b back to rotation matrices using Eq. 3. In this work, we formulated the optimization problem using unit quaternions and solved with a commercial numerical solver. However, alternative methods, such as using manifold structure of rotation groups [28], [29], may also be used to solve Eq. 2 analytically.

B. Methods for Comparison (GOM and GYLM)

For evaluating SAM, we designed two other alignment methods using common assumptions from literature, which we refer to as the 'Global Only Method' (GOM) and 'Global Yaw + Local Method' (GYLM). We developed custom methods as baselines, instead of using existing ones from literature. This is because existing methods have different calibration procedures with varying levels of complexity, and may use more than just orientation information, which are difficult to replicate and ensure fair comparison. Additionally, most existing methods separate the local and global frame alignment issues and do not solve our target problem of simultaneous alignment of both frames.

1) Global Only Method (GOM): In GOM, we assume that the local frames of IMU and OMC are identical. This is a common assumption used in literature [11], [21] as the IMU chip and its physical case are often manually aligned and rigidly fixed. The alignment precision may vary, but for simplicity, the local frame alignment rotation is assumed to be identity,

$$R_{OL_{\text{GOM}}}^{IL} = I. \tag{8}$$

For the global frame alignment, we find the rotational differences between the OMC and IMU orientations and then take the mean across all time points,

$$R_{IG_{\text{GOM}}}^{OG} = \underset{t\in[0,T]}{\text{mean}}(R_{OL,t}^{OG} R_{IL,t}^{IG\ T}) \tag{9}$$

where R^T represents the transpose of a rotation matrix R. Averaging 3D rotations can be achieved using unit quaternion representation.

2) Global Yaw + Local Method (GYLM): In GYLM, we acknowledge that both local and global frame alignments are required, but with the assumption that the global frame mismatch is in the yaw direction *only*. This assumption is made because the main contributor of global frame mismatch is the inconsistency between the magnetic north and the OMC lab heading in the x–y plane. Additionally, due to an IMU magnetometer's dependence on initial factory settings and local magnetic fields in the testing environment, more errors in yaw may occur [20], [30]. We developed this custom baseline method as it aligns both global and local frames, while existing methods [19], [21], [23] address local and global alignments independently.

GYLM can be solved in close form by first decomposing the global alignment rotation from the GOM method from Eq. 9 into sequential rotations of yaw, pitch and roll,

$$R_{IG_{\text{GOM}}}^{OG} = R_z(\psi)R_y(\theta)R_x(\phi) \tag{10}$$

where ψ, θ, ϕ are yaw, pitch, and roll angles about z, y, x axes respectively.

In GYLM, the global frame alignment is found by taking only the yaw component of Eq. 10 using

$$R_{IG_{\text{GYLM}}}^{OG} = R_z(\psi). \tag{11}$$

The local frame alignment is then found by applying the global frame alignment and averaging the remaining rotational differences across all time points:

$$R_{OL_{\text{GYLM}}}^{IL} = \underset{t\in[0,T]}{\text{mean}}((R_{IG_{\text{GYLM}}}^{OG} R_{IL,t}^{IG})^T R_{OL,t}^{OG}). \tag{12}$$

IV. Protocol and Metrics

A. Experimental Setup and Protocol

We collected arm movement data from 6 human participants to validate the methods' performance. The data collection was performed under Harvard Institutional Review Board (Protocol IRB19-1321) and all participants were consented. For each participant, we placed 3 IMUs (MTi-3 series, XSens Technologies, Netherlands) on their torso and left and right upper arms, as shown in Fig. 2A. Each IMU was mounted on a custom 3D printed case with 4 OMC markers on each of the corners, captured by 29 OMC cameras (Qualisys, Sweden). Data from IMUs and OMC were logged and synced using a real-time target machine (Speedgoat, Switzerland).

For each participant, two types of motion data were collected, as illustrated in Fig. 2B. First, we asked the participants to perform short cyclic motions of shoulder forward flexion/extension (FF), abduction/adduction (AB), horizontal flexion/extension (HF), and internal/external rotation (IR). IR was performed with arms by the side and elbows bent. The participants performed three repetitions of each motion in their comfortable angle ranges. This cyclic motion sequence took approximately 40 seconds on average. Next, we asked participants to perform a long duration functional motion trial. The participants performed overhead drilling, desk work (such as typing and note-taking), treadmill walking, and random arm motions. The drilling, desk work, and walking tasks were

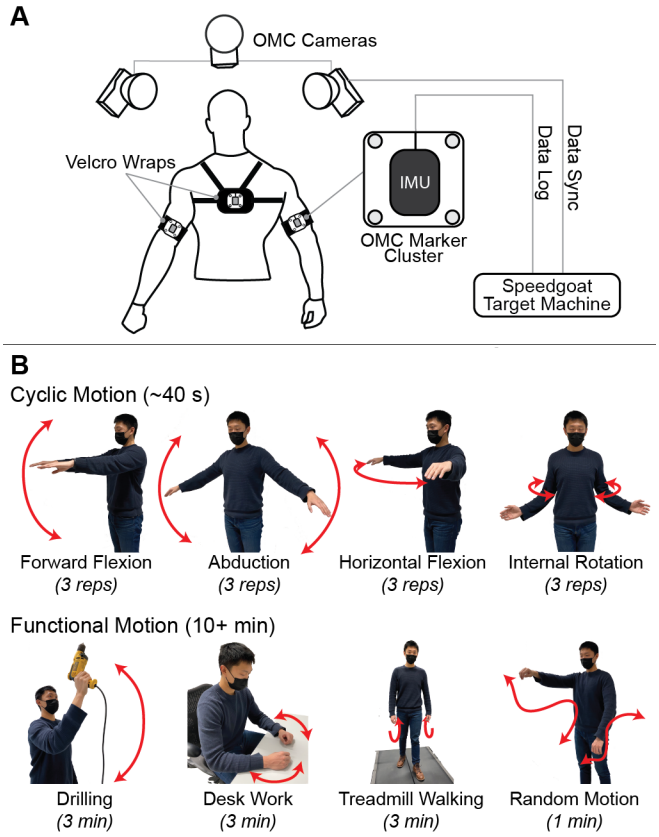

Fig. 2. (A) Illustration of experimental setup including a human participant wearing IMUs on torso and arms in a motion capture lab. (B) Photos of motion performed during short duration cyclic motion trial and long duration functional motion trial.

3 minutes each and the random motion was 1 minute. The trial totaled over 10 minutes including transition time among the tasks.

B. Evaluation Metrics

We used the root-mean-square error (RMSE) and the Pearson's correlation coefficient as the key evaluation metrics to assess the performance of different alignment techniques described in Section III. To calculate these metrics, we first define the following time series profiles using angular distance.

1) Time Series Profiles: Angular distance is the minimal rotation angle that aligns one 3D rotation to another as used by Huynh [31]. Between two rotation matrices, R_1 and R_2, angular distance, θ, can be found using

$$\theta = \arccos\left(\frac{\mathrm{tr}(R_1^T R_2) - 1}{2}\right) \tag{13}$$

where $\mathrm{tr}(X)$ represents taking the trace of a matrix X.

In this work, Eq. 13 is used for representing time series error and motion magnitude profiles.

- Time series *error profiles* are calculated by finding the angular distances between the aligned IMU orientations and the OMC ground truth orientations. Specifically, at each time frame, t, the error is calculated using Eq. 13 with

$$\begin{aligned} R_{1,t} &= R_{IG}^{OG} R_{IL,t}^{IG} R_{OL}^{IL}, \\ R_{2,t} &= R_{OL,t}^{OG} \end{aligned} \tag{14}$$

  where $R_{1,t}$ represents the aligned IMU orientations as described in Section II and III and $R_{2,t}$ represents the OMC measurements.
- Time series *motion magnitude profiles* are calculated using Eq. 13 with

$$\begin{aligned} R_{1,t} &= R_{OL,0}^{OG}, \\ R_{2,t} &= R_{OL,t}^{OG} \end{aligned} \tag{15}$$

  where $R_{1,t}$ represents the OMC orientation at the initial time frame of a motion trial and $R_{2,t}$ represents the OMC orientation at each time frame, t. We use this calculation to represent 3D motions with a 1D magnitude profile, both for qualitative motion visualization and quantitative evaluation metrics calculation.

2) RMSE & Pearson's Correlation Coefficient: Our main evaluation metrics for frame alignment are RMSEs and Pearson's correlation coefficients. We use RMSE of the time series error profile to evaluate frame alignment accuracy. Comparing among the alignment methods, the one that generates the lowest RMSE has the highest alignment accuracy.

We use Pearson's correlation coefficients to quantify the correlation between the time series error and motion magnitude profiles. If the local and global frames between an IMU and an OMC are accurately aligned, the error profile should be independent from the motion magnitude profile, because the alignment accuracy should not vary with where the IMU is in space. Hence, a lower correlation coefficient suggests a better alignment method. There is a large range of interpretations of correlation coefficient to their labelled strength of correlation [32]. Based on general guidelines, we view coefficient values less than 0.3 as weak correlation, between 0.3 and 0.5 as moderate correlation, and greater than 0.5 as strong correlation.

V. Performance Evaluation

To evaluate the performance of SAM, we used data from the short cyclic motion trials from all participants and compared its performance to that of the simplified methods, GOM and GYLM (Section III.B). The alignment rotations were fitted and evaluated using data from the whole cyclic motion trial. We computed both the RMSE and the Pearson's correlation coefficient for evaluation and pooled the results from all participants to account for the variance across different participants, motions, and testing days. The multi-participant results are presented in Table I and II.

Compared to GOM and GYLM, SAM generated the lowest RMSEs, below 1.5° on average, for all participants across all 3 IMU locations. We saw mostly weak correlation between motion and error for SAM while moderate to high correlations for GOM and GYLM. These results show the better performance of the proposed method, which highlights the advantage of simultaneously aligning both local and global

TABLE I

FRAME ALIGNMENT ACCURACY (RMSE)

IMU Location	SAM	GYLM	GOM
Torso	**0.64° ± 0.54°**	0.71° ± 0.54°	0.75° ± 0.53°
Left Arm	**1.06° ± 0.14°**	3.20° ± 1.38°	7.32° ± 1.13°
Right Arm	**1.49° ± 0.45°**	3.04° ± 0.56°	7.16° ± 0.99°

TABLE II

CORRELATION BETWEEN ALIGNMENT ERROR AND MOTION MAGNITUDE (PEARSON'S CORRELATION COEFFICIENTS)

IMU Location	SAM	GYLM	GOM
Torso	**0.32 ± 0.17**	0.48 ± 0.17	0.52 ± 0.16
Left Arm	**0.26 ± 0.05**	0.57 ± 0.16	0.80 ± 0.05
Right Arm	**0.18 ± 0.12**	0.65 ± 0.14	0.71 ± 0.12

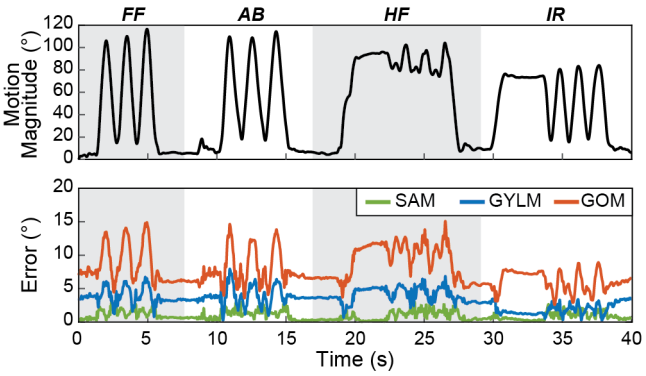

Fig. 3. Example time series plots of the arm motion magnitude profile (top) and the error profiles from the 3 alignment methods (bottom). Data is collected from one participant during the cyclic motion trial. Compared to the other two methods, the proposed alignment method (in green) generates the lowest error with error profile the least correlated to the motion magnitude.

frames and not relying on common assumptions, such as *perfect* sensor-to-case alignment or global misalignment in yaw direction *only*. When comparing within the assumption-based methods, GYLM outperforms GOM with lower RMSEs and correlation coefficients, indicating that in this scenario the assumption made by GYLM is better than the one by GOM.

It is interesting to compare the performance of the torso IMU to those of the arm IMUs. For all three methods, RMSE of torso IMU is lower than those of the arm IMUs. Comparing across methods, SAM has much lower absolute and percentage RMSE reduction (compared to GYLM and GOM) for torso than for arm IMUs. Lastly, for SAM, the correlation coefficient for torso IMU is higher and more variable than for arm IMUs. Such discrepancy between the torso IMU and the arm IMUs is likely because the torso IMU goes through a much smaller range of motion during the trials. The effect of range of motion on alignment quality is studied more in detail in the following section.

To visualize the alignment performances, Fig. 3 shows a time series example of an arm IMU's motion with the corresponding error profiles from the 3 methods. The motion and error profiles are defined using angular distance in Section IV.B. The top plot shows the motion magnitude profile, which can be interpreted as the magnitude of the arm IMU rotation during the trial relative to the initial arms-down position. Using this magnitude-only representation, we can better see if the error profile is correlated with the motion. The bottom error plot reflects the results from Tables I and II, with SAM having the lowest error and least correlated error profile. It is interesting to note that residual errors are higher during the dynamic regions than the static ones. These remaining errors after applying SAM are likely due to IMU and OMC measurement noises, with greater inconsistencies during dynamic motions.

VI. SENSITIVITY ANALYSIS

Because SAM is an optimization based method, its alignment accuracy is affected by the input data. Specifically, we hypothesize that, if the input data contains a more diverse set of rotations, SAM could find more accurate alignment matrices.

To understand how the range of motion of the input data affects the algorithm performance, we performed a sensitivity analysis to explore the relationship between alignment accuracy and the averaged pairwise angular distance (APAD). Specifically, for a set of 3D rotations, APAD is calculated by (1) computing the angular distances between each unique pair of rotations using Eq. 13 and (2) taking the average of all pairwise angular distances. This pairwise metric serves as a proxy for range of motion as it not only quantifies the *magnitude* of motion present in the dataset, but also accounts for the *directionality*. For instance, orientations clustered about a single axis of rotation will yield a lower APAD value than rotations about multiple axes.

To perform sensitivity analysis, we used data from both arm IMUs during cyclic motion trials for all participants. We broke the trials into non-overlapping windows, ranging from 0.5 seconds to 40 seconds. We used the data within each window to fit alignment rotations and used the corresponding full trial data to measure the alignment accuracy. APAD of each window was then calculated and evaluated against the alignment accuracy.

Fig. 4 shows the range of motion sensitivity analysis results from the 3 methods. The performance of GOM and GYLM stay mostly constant, whereas that of SAM drastically improves with larger APAD. This trend is expected for an optimization based method as more diverse data would allow more accurate fit that can better explain the alignment discrepancies throughout the entire trial. We then used paired t-tests to evaluate the statistical significance in the distribution difference between SAM and GOM and between SAM and GYLM. Quantitatively, SAM has higher error ($p < 0.05$) than GOM for APAD $< 3.2°$ and GYLM for APAD $< 8.2°$. This relationship is reversed with larger APAD where SAM outperforms ($p < 0.05$) GOM for APAD $> 4.1°$ and GYLM for APAD $> 11.4°$. Compared to GOM and GYLM, SAM has more unknown parameters to fit and thus is more likely to

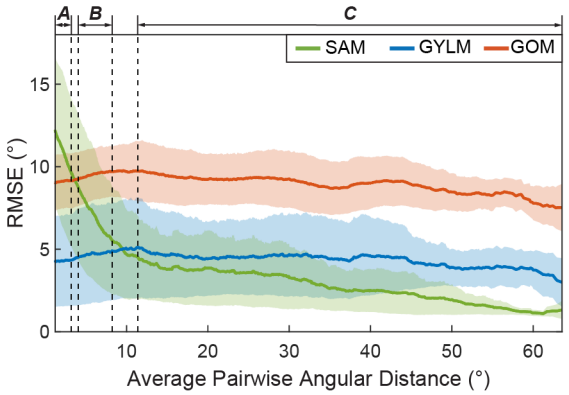

Fig. 4. Sensitivity analysis showing how alignment accuracy (RMSE) is affected by average pairwise angular distance (APAD). We applied a moving window of 7.5° APAD to get the mean (solid line) and the mean absolute deviation (shaded region). In region A (APAD $< 3.2°$), SAM has higher error than both GOM and GYLM. In region B ($4.1° <$ APAD $< 8.2°$), SAM has higher error than GYLM but lower error than GOM. In region C (APAD $> 11.4°$), SAM has lower error than both GOM and GYLM. These cutoffs were identified using paired t-tests with $p < 0.05$.

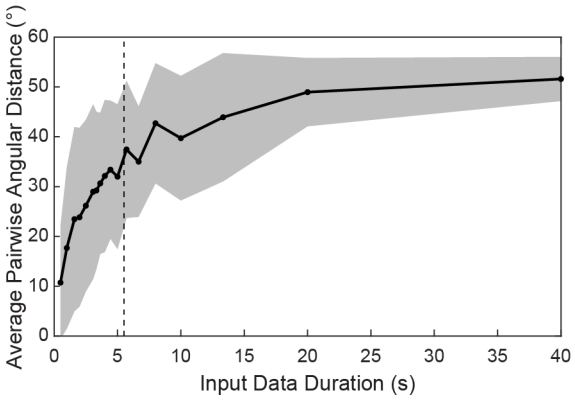

Fig. 5. The relationship between average pairwise angular distance (APAD) and input data time duration for our shoulder motion dataset, showing longer data duration leads to higher APAD. The solid line represents the means at the different durations and the shaded region represents the standard deviations. The vertical dashed line at 5.5 seconds indicates the time duration with the corresponding APAD greater than 11.4° with 95% confidence (z-score of 1.64). The 11.4° APAD cutoff is identified in Fig. 4 region C at which SAM is more accurate than GOM and GYLM. This indicates that, for our dataset, with input data duration greater than 5.5 seconds, SAM outperforms the other methods.

overfit when the input data is unrepresentative of all possible orientations. However, with data covering enough diversity in orientation, an assumption-free method, like SAM, can achieve better performance than the assumption-based ones.

We also conducted a similar analysis to understand the relationship between Pearson's correlation coefficient and APAD. Unlike RMSE, however, the correlation coefficient did not exhibit any discernible trend as a function of APAD for any of the three methods. This suggests that while the *magnitude* of the error decreased when SAM was exposed to more diverse data, the *shape* of the time series error profile remained relatively consistent. That said, SAM still exhibited a lower average correlation coefficient than GOM and GYLM (as shown in Table II).

Lastly, we evaluated the relationship between the input data duration and the range of motion by plotting the input data duration versus APAD. As shown in Fig. 5, the mean of APAD increases with the input data duration. To find the minimum acceptable duration for which SAM outperforms the other methods in our dataset, we first identify an APAD threshold of 11.4° from Fig. 4 at which SAM starts to show more accurate alignment than GOM and GYLM. From Fig. 5, we then identified time duration greater than 5.5 seconds would correspond APAD values larger than the 11.4° threshold

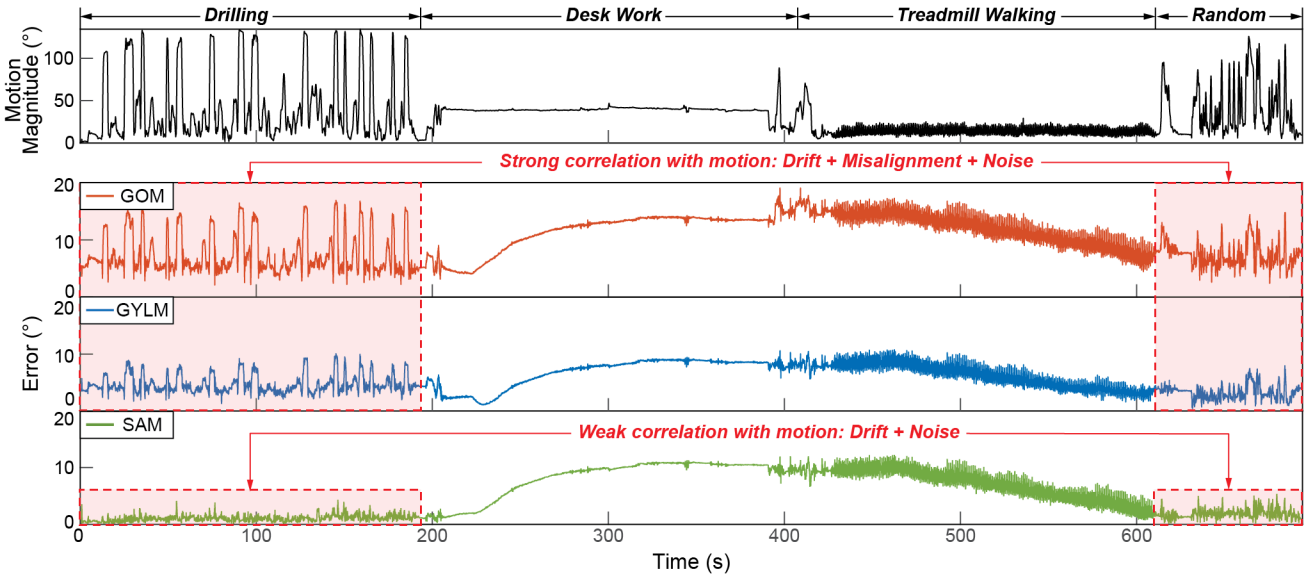

Fig. 6. Example time series plots for arm motion magnitude profile (top) and alignment error profiles (bottom) from three methods. Compared to GOM (orange) and GYLM (blue), SAM (green) shows least motion correlated errors, especially during dynamic tasks (drilling and random motion). The weak correlation indicates that SAM can isolate drift from misalignment errors, which is important for understanding IMU drift behaviors.

with $> 95\%$ confidence (z-score of 1.64). This indicates that for our specific dataset, applying SAM with greater than 5.5 seconds of data would generate more accurate alignment matrices than GOM and GYLM. Although the specific duration cutoff is a characteristic of our particular dataset, comparable short duration values are expected to be seen for data with different arm motions.

VII. Drift Isolation Demonstration

IMU drift is a widely known issue that occurs from integrating noisy gyroscope signals. It is a slowly accumulated error, especially difficult to visualize during dynamic motion. Isolating and visualizing errors due to drift is important for understanding sensor behaviors in different environments and developing corrective measures.

In this final section, we demonstrate that SAM can better isolate and visualize IMU drift compared to GOM and GYLM, which aids in algorithm development for correcting yaw drift. For this demonstration, we used data from one participant. The alignment rotations were found using the entire short cyclic motion data from that participant and were applied to the long duration functional motion data. We visualized the pattern of the drift using the time series error profile.

Fig. 6 shows the time series motion magnitude profile and the corresponding error profiles from the three methods. Among all methods, SAM resulted in an error profile least correlated with the motion, especially for drilling and random motions. With GOM and GYLM, the error profiles during those dynamic tasks are highly correlated with motion. Specifically, for those dynamic tasks, SAM has a Pearson's correlation coefficient of 0.04, whereas those of GYLM and GOM are 0.74 and 0.88 respectively. These motion-correlated errors are more likely to be from misalignment as opposed to drift, because we expect drift to behave like a low frequency signal. All three alignment methods result in similar drift trends during the more static, low-motion-magnitude tasks: desk work and treadmill walking. It is interesting to note that during treadmill walking, all three methods show highly noisy errors. One possibility for this observation is that there was more marker occlusion from the OMC in our specific treadmill setup.

With the proposed alignment method, the notorious IMU drift can be isolated and visualized especially during dynamic movements. This capability is valuable for understanding drift behaviors and developing IMU de-drifting algorithms.

VIII. Conclusion

We proposed a method for simultaneously aligning the global and local frames between an IMU and an OMC system. We demonstrated its greater alignment performance over methods requiring various simplifying assumptions common in literature. In addition, we showed through sensitivity analysis the importance of using input data with diverse set of rotations to ensure alignment accuracy. Lastly, we demonstrated the method's capability of isolating and visualizing IMU drift during dynamic motions, which is difficult to achieve as any frame misalignment errors can convolute with drift errors and hinder our ability to study drift on its own. The proposed data-based and assumption-free method serves as a valuable tool for evaluating and developing IMU algorithms, such as de-drifting techniques for long term motion tracking.

Appendix: Simplifying the Residual Function

To simplify the least squares residual function, ρ, from Eq. 5, we use quaternion properties of $\|q\| = qq^*$, $(pq)^* = q^*p^*$, $qq^* = 1$, and $q + q^* = 2[q]_S$, where q and p are two quaternions and $[q]_S$ represents the scalar component of q.

Eq. 5 simplifies to Eq. 6 by

$$\begin{aligned}
\rho &= \sum_{t=0}^{T} \|u_t a - b w_t\|^2 \\
&= \sum_{t=0}^{T} (u_t a - b w_t)(u_t a - b w_t)^* \\
&= \sum_{t=0}^{T} (u_t a a^* u_t^* + b w_t w_t^* b^* - b w_t a^* u_t^* - u_t a w_t^* b^*) \\
&= \sum_{t=0}^{T} (1 + 1 - 2[b w_t a^* u_t^*]_S) \\
&= 2(T+1) - 2\sum_{t=0}^{T} [b w_t a^* u_t^*]_S.
\end{aligned}$$

References

[1] J. K. Aggarwal and Q. Cai, "Human motion analysis: A review," *Computer vision and image understanding*, vol. 73, no. 3, pp. 428–440, 1999.

[2] H. Zhou and H. Hu, "Human motion tracking for rehabilitation—a survey," *Biomedical signal processing and control*, vol. 3, no. 1, pp. 1–18, 2008.

[3] Y. M. Zhou, C. Hohimer, T. Proietti, C. T. O'Neill, and C. J. Walsh, "Kinematics-based control of an inflatable soft wearable robot for assisting the shoulder of industrial workers," *IEEE Robotics and Automation Letters*, vol. 6, no. 2, pp. 2155–2162, 2021.

[4] T. Proietti, C. O'Neill, C. J. Hohimer, K. Nuckols, M. E. Clarke, Y. M. Zhou, D. J. Lin, and C. J. Walsh, "Sensing and control of a multi-joint soft wearable robot for upper-limb assistance and rehabilitation," *IEEE Robotics and Automation Letters*, vol. 6, no. 2, pp. 2381–2388, 2021.

[5] Y. Jin, C. M. Glover, H. Cho, O. A. Araromi, M. A. Graule, N. Li, R. J. Wood, and C. J. Walsh, "Soft sensing shirt for shoulder kinematics estimation," in *2020 IEEE International Conference on Robotics and Automation (ICRA)*. IEEE, 2020, pp. 4863–4869.

[6] M. Kok and T. B. Schön, "A fast and robust algorithm for orientation estimation using inertial sensors," *IEEE Signal Processing Letters*, vol. 26, no. 11, pp. 1673–1677, 2019.

[7] I. Weygers, M. Kok, H. De Vroey, T. Verbeerst, M. Versteyhe, H. Hallez, and K. Claeys, "Drift-free inertial sensor-based joint kinematics for long-term arbitrary movements," *IEEE Sensors Journal*, vol. 20, no. 14, pp. 7969–7979, 2020.

[8] R. G. Valenti, I. Dryanovski, and J. Xiao, "A linear Kalman filter for marg orientation estimation using the algebraic quaternion algorithm," *IEEE Transactions on Instrumentation and Measurement*, vol. 65, no. 2, pp. 467–481, 2015.

[9] S. O. Madgwick, A. J. Harrison, and R. Vaidyanathan, "Estimation of IMU and MARG orientation using a gradient descent algorithm," in *2011 IEEE International Conference on Rehabilitation Robotics*. IEEE, 2011, pp. 1–7.

[10] B. Bouvier, S. Duprey, L. Claudon, R. Dumas, and A. Savescu, "Upper limb kinematics using inertial and magnetic sensors: Comparison of sensor-to-segment calibrations," *Sensors*, vol. 15, no. 8, pp. 18 813–18 833, 2015.

[11] P. Picerno, P. Caliandro, C. Iacovelli, C. Simbolotti, M. Crabolu, D. Pani, G. Vannozzi, G. Reale, P. M. Rossini, L. Padua *et al.*, "Upper limb joint kinematics using wearable magnetic and inertial measurement units: an anatomical calibration procedure based on bony landmark identification," *Scientific reports*, vol. 9, no. 1, pp. 1–10, 2019.

[12] T. Seel, J. Raisch, and T. Schauer, "IMU-based joint angle measurement for gait analysis," *Sensors*, vol. 14, no. 4, pp. 6891–6909, 2014.

[13] A. Filippeschi, N. Schmitz, M. Miezal, G. Bleser, E. Ruffaldi, and D. Stricker, "Survey of motion tracking methods based on inertial sensors: A focus on upper limb human motion," *Sensors*, vol. 17, no. 6, p. 1257, 2017.

[14] H. Kainz, L. Modenese, D. Lloyd, S. Maine, H. Walsh, and C. Carty, "Joint kinematic calculation based on clinical direct kinematic versus inverse kinematic gait models," *Journal of biomechanics*, vol. 49, no. 9, pp. 1658–1669, 2016.

[15] B. Fan, Q. Li, T. Tan, P. Kang, and P. B. Shull, "Effects of IMU sensor-to-segment misalignment and orientation error on 3D knee joint angle estimation," *IEEE Sensors Journal*, 2021.

[16] G. Wu, S. Siegler, P. Allard, C. Kirtley, A. Leardini, D. Rosenbaum, M. Whittle, D. D D'Lima, L. Cristofolini, H. Witte *et al.*, "ISB recommendation on definitions of joint coordinate system of various joints for the reporting of human joint motion—part I: ankle, hip, and spine," *Journal of Biomechanics*, vol. 35, no. 4, pp. 543–548, 2002.

[17] G. Wu, F. C. Van der Helm, H. D. Veeger, M. Makhsous, P. Van Roy, C. Anglin, J. Nagels, A. R. Karduna, K. McQuade, X. Wang *et al.*, "ISB recommendation on definitions of joint coordinate systems of various joints for the reporting of human joint motion—part II: shoulder, elbow, wrist and hand," *Journal of Biomechanics*, vol. 38, no. 5, pp. 981–992, 2005.

[18] P. Arens, C. Siviy, J. Bae, D. K. Choe, N. Karavas, T. Baker, T. D. Ellis, L. N. Awad, and C. J. Walsh, "Real-time gait metric estimation for everyday gait training with wearable devices in people poststroke," *Wearable Technologies*, vol. 2, 2021.

[19] H. Mecheri, X. Robert-Lachaine, C. Larue, and A. Plamondon, "Evaluation of eight methods for aligning orientation of two coordinate systems," *Journal of biomechanical engineering*, vol. 138, no. 8, 2016.

[20] W. De Vries, H. Veeger, C. Baten, and F. Van Der Helm, "Magnetic distortion in motion labs, implications for validating inertial magnetic sensors," *Gait & posture*, vol. 29, no. 4, pp. 535–541, 2009.

[21] E. Bergamini, P. Guillon, V. Camomilla, H. Pillet, W. Skalli, and A. Cappozzo, "Trunk inclination estimate during the sprint start using an inertial measurement unit: A validation study," *Journal of applied biomechanics*, vol. 29, no. 5, pp. 622–627, 2013.

[22] Xsens, *MTw Awinda User Manual*, Xsens, Enschede, Netherlands, May 2018.

[23] J. K. Lee and W. C. Jung, "Quaternion-based local frame alignment between an inertial measurement unit and a motion capture system," *Sensors*, vol. 18, no. 11, p. 4003, 2018.

[24] J. Chardonnens, J. Favre, and K. Aminian, "An effortless procedure to align the local frame of an inertial measurement unit to the local frame of another motion capture system," *Journal of biomechanics*, vol. 45, no. 13, pp. 2297–2300, 2012.

[25] Z. Song, Z. Cao, Z. Li, J. Wang, and Y. Liu, "Inertial motion tracking on mobile and wearable devices: Recent advancements and challenges," *Tsinghua Science and Technology*, vol. 26, no. 5, pp. 692–705, 2021.

[26] F. Wittmann, O. Lambercy, and R. Gassert, "Magnetometer-based drift correction during rest in IMU arm motion tracking," *Sensors*, vol. 19, no. 6, p. 1312, 2019.

[27] M. Topley and J. G. Richards, "A comparison of currently available optoelectronic motion capture systems," *Journal of Biomechanics*, vol. 106, p. 109820, 2020.

[28] C. Forster, L. Carlone, F. Dellaert, and D. Scaramuzza, "Imu preintegration on manifold for efficient visual-inertial maximum-a-posteriori estimation." Georgia Institute of Technology, 2015.

[29] D. Kim, S. Shin, and I. S. Kweon, "On-line initialization and extrinsic calibration of an inertial navigation system with a relative preintegration method on manifold," *IEEE Transactions on Automation Science and Engineering*, vol. 15, no. 3, pp. 1272–1285, 2017.

[30] M. Iosa, P. Picerno, S. Paolucci, and G. Morone, "Wearable inertial sensors for human movement analysis," *Expert review of medical devices*, vol. 13, no. 7, pp. 641–659, 2016.

[31] D. Q. Huynh, "Metrics for 3D rotations: Comparison and analysis," *Journal of Mathematical Imaging and Vision*, vol. 35, no. 2, pp. 155–164, 2009.

[32] H. Akoglu, "User's guide to correlation coefficients," *Turkish journal of emergency medicine*, vol. 18, no. 3, pp. 91–93, 2018.